Synthesis of Directly Linked Zinc(II) Porphyrin–Imide Dyads and Energy Gap Dependence of Intramolecular Electron Transfer Reactions

Naoya Yoshida,[a] Tomoya Ishizuka,[a] Katsuyuki Yofu,[a] Masataka Murakami,[b] Hiroshi Miyasaka,*[b] Tadashi Okada,[b] Yasushi Nagata,[c] Akira Itaya,[c] Hyun Sun Cho,[d] Dongho Kim,*[d] and Atsuhiro Osuka*[a]

Abstract: A series of zinc(II) porphyrin–imide dyads (**ZP-Im**), in which an electron donating ZP moiety is *directly* connected to an electron accepting imide moiety in the *meso* position, have been prepared for the examination of energy gap dependence of intramolecular electron transfer reactions with large electronic coupling. The nearly perpendicular conformation of the imide moiety towards the porphyrin plane has been revealed by X-ray crystal structures. The energy gap for charge separation, ^{1}**ZP*–Im** → **ZP$^+$–Im$^-$**, is varied by changing the electron accepting imide moiety to cover a range of about 0.8 eV in DMF. Definitive evidence for electron transfer has been obtained in three solvents (toluene, THF, and DMF) through picosecond–femtosecond transient absorption studies, which have allowed us to determine the rates of photoinduced charge separation, ^{1}**ZP*–Im** → **ZP$^+$–Im$^-$**, and subsequent thermal charge recombination **ZP$^+$–Im$^-$** → **ZP–Im**. The free-energy gap dependence (energy gap law) has been probed from the normal to the nearly top region for the charge separation rate alone, and only the inverted region for the charge recombination rate. Although both of the energy gap dependencies can be approximately reproduced by means of the simplified semiclassical equation, when we take into consideration the effect of the high frequency vibrations replaced by one mode of averaged frequency, many features, including the effects of solvent polarity and the electron tunneling matrix element on the energy gap law, differ considerably from those of the previously studied porphyrin–quinone systems, which have weaker interchromophore electronic interactions.

Keywords: absorption · donor–acceptor systems · electron transfer · porphyrinoids

Introduction

Among many factors that govern electron transfer (ET) reactions, the free energy gap ($-\Delta G$) dependence of the ET rate (energy-gap law) has been extensively studied with the goal of confirming the Marcus theory,[1] and thus to deepen the understanding of fundamental mechanisms of ET. Distance-fixed covalently-linked donor–acceptor pairs are particularly effective in examining the energy gap law, since such models are free from concerns about donor-acceptor distance distribution.[2] Most models so far examined have been limited to those with weak electronic coupling between the donor and acceptor, since the Marcus Equation [Eq. (1)] is valid in nonadiabatic regimes.[3, 4] In this expression, V is the electronic tunneling matrix element, and FCWD represents the nuclear coordinates as the Franck–Condon weighted density of states.[1b] FCWD depends on the energy gap, the nuclear vibrational modes relevant to the ET process, the changes in bond lengths and angles of the substrates and the changes in solvation upon ET.

$$k_{ET} = \frac{2\pi}{\hbar} V^2 \,\mathrm{FCWD} \qquad (1)$$

[a] Prof. A. Osuka, N. Yoshida, T. Ishizuka, K. Yofu
Department of Chemistry, Graduate School of Science
Kyoto University, Kyoto 606-8502 (Japan)
and Core Research for Evolutional Science and Technology (CREST)
of Japan Science and Technology Corporation (JST)
Fax: (+81) 75-753-3970
E-mail: osuka@kuchem.kyoto-u.ac.jp

[b] Prof. H. Miyasaka, M. Murakami, Prof. T. Okada
Department of Chemistry, Graduate School of Technology
Osaka University, Osaka 550 (Japan)

[c] Y. Nagata, Prof. A. Itaya
Department of Polymer Science and Engineering, Kyoto Institute of Technology
Kyoto 606-8585 (Japan)

[d] Prof. D. Kim, Dr. H. S. Cho
National Creative Research Initiatives Center
for Ultrafast Optical Characteristics Control
and Department of Chemistry
Yonsei University, Seoul 120-749 (Korea)

Supporting information for this article containing the X-ray crystal structures of **ZP-MPH**, **ZP-Cl$_2$PH**, and **ZP-Cl$_4$PH** and fluorescence decay profiles of **ZP-PH** and **ZP-ClPH** in THF and **ZP-PH** in DMF and their biexponential fits is available on the WWW under http://www.chemeurj.org/ or from the author.

DOI: 10.1002/chem.200204588

Through our own studies on the energy-gap law,[4–7] we became interested in testing the Marcus theory in a region of rather large electronic coupling. This interest stems from a recent finding that the energy-gap law of charge recombination in contact ion pairs follows a so-called exponential energy-gap law of $k_{CR} = \exp[-\beta\,|\,\Delta G_{CR}\,|\,]$.[7] With this in mind, we designed a new class of Zn^{II} porphyrin-imide acceptor models (**ZP-Im**)[8] (Scheme 1) to examine the

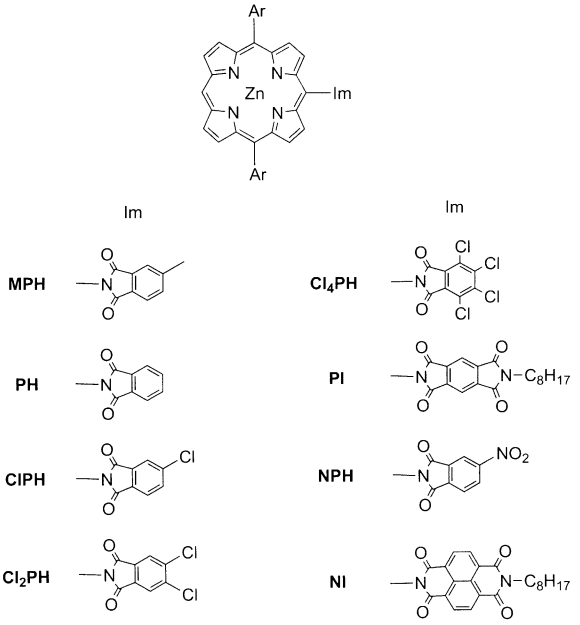

Scheme 1.

energy-gap law in a region of large electronic coupling. A key structural feature of **ZP-Im** is the *direct* linkage of an electron-accepting imide at the *meso* position of Zn^{II} porphyrin, where a rather restricted perpendicular arrangement is likely to minimize the electronic interactions. Another important feature is the easy detection of anion radicals, particularly for pyromellitimide (**PI**) and 1,8:4,5-naphthalene-tetracarboxylic diimide (**NI**).[9] Using these **ZP-Im** dyads, we recently revealed a bell-shaped energy-gap dependence for the charge separation (CS) between the S_2-excited state of **ZP** and **Im** as the first unambiguous demonstration of CS reactions in covalently-linked systems.[10] This success seems to arise from the wide energy gap available for the CS process and the relatively long-lived S_2 state of Zn^{II} TPP-type porphyrins.[11]

The present models may also be attractive in light of their ultrafast ET, since such molecules may be of use in molecular devices such as switches[12] and logic gates,[13] which preferably have ultrafast response and integration. In these applications, the prediction of ET rates based on a reliable theory is of the utmost importance in the design of the molecular devices. As closely related donor-acceptor molecules, there have been many examples of directly linked porphyrin-quinone dyads,[14, 15] most of which exhibit characteristic charge transfer (CT) absorption bands that reflect much stronger electronic coupling. Among these, it is interesting to note that Hochstrasser and Therien reported the occurrence of CS between the vibrationally hot S_1 state of Mg^{II} porphyrin and benzoquinone.[15]

Here, we report the synthesis and characterization of *directly* linked Zn^{II} porphyrin-imide molecules (**ZP-Im**). Particular attention is focused on the energy-gap dependence of the CS ^{1}**ZP*–Im** → **ZP**$^+$**–Im**$^-$ and subsequent thermal charge recombination (CR) **ZP**$^+$**–Im**$^-$ → **ZP–Im** in situations with quite large electronic coupling.

Results and Discussion

Synthesis: Directly linked porphyrin-imide dyads were prepared from the condensation of Zn^{II} 10-amino-5,15-bis(3,5-di-*tert*-butylphenyl)porphyrin (**ZPNH$_2$**) and corresponding dicarboxylic anhydrides (Scheme 2). Treatment of Zn^{II} 5,15-bis(3,5-di-*tert*-butylphenyl)porphyrin (**ZDP**) with $AgNO_2$ and

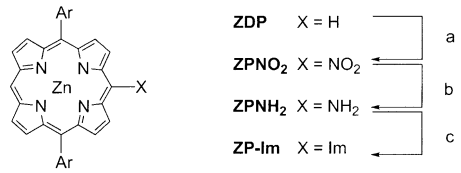

Scheme 2.

I_2 in $CHCl_3$ gave Zn^{II} 10-nitro-5,15-bis(3,5-di-*tert*-butylphenyl)porphyrin (**ZPNO$_2$**) in 98% yield.[16, 17] This was reduced with $SnCl_2$/HCl and remetallated with $Zn(OAc)_2$ to give Zn^{II} 10-amino-5,15-bis(3,5-di-*tert*-butylphenyl)porphyrin (**ZPNH$_2$**) in 87% yield.[16] The Zn^{II} porphyrin-imide dyads (**ZP-Im**) were prepared by the condensation of **ZPNH$_2$** and the corresponding anhydrides in 6–48% yield by heating in pyridine or DMF, although the reaction conditions (solvent, concentration, temperature, and reaction time) were adjusted depending on the structures of anhydrides.

In the reaction with 3,4,5,6-tetrafluorophthalic anhydride, the corresponding porphyrin-imide was not obtained but porphyrin-tetrafluorophenylcarboxyamide was isolated in low yield (3%, **ZP-F$_4$PA**, Scheme 3). Diimide-linked Zn^{II}

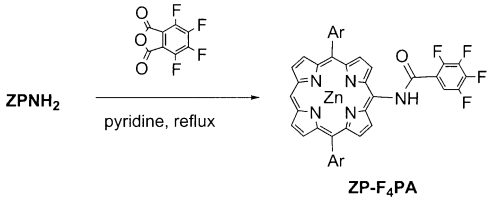

Scheme 3.

porphyrins **ZP-PI** and **ZP-NI** were prepared by the condensation of **ZPNH$_2$** with half imides **1** and **2**, respectively (Scheme 4). This condensation achieved 44% yield for **ZP-PI**, which is higher than the yield (12%) reported for the cross condensation reaction.[8]

Alternatively, we found that **ZP-Im** can be prepared directly from nucleophilic trapping of the Zn^{II} porphyrin

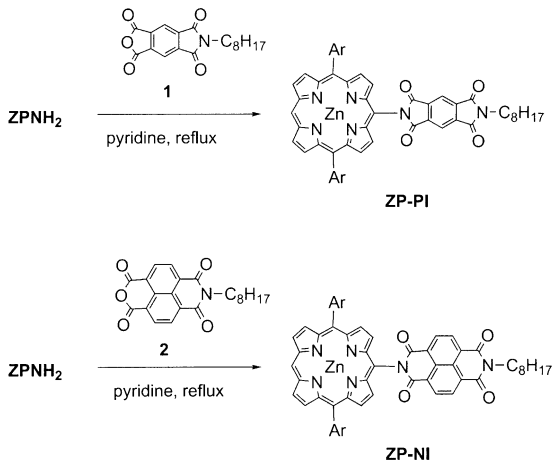

Scheme 4.

cation radical by a phthalimide anion. Addition of $(BrC_6H_4)_3NSbCl_6$ to a solution containing **ZDP**, [18]crown-6, and excess potassium phthalimide in $CHCl_3$ resulted in direct coupling of a phthalimide moiety at the *meso* position of Zn^{II} porphyrin to afford **ZP-PH** (35%) with concurrent formation of *meso*–*meso* linked oligoporphyrins[17] as byproducts (Scheme 5). Dyad **ZP-MPH** was similarly prepared by the

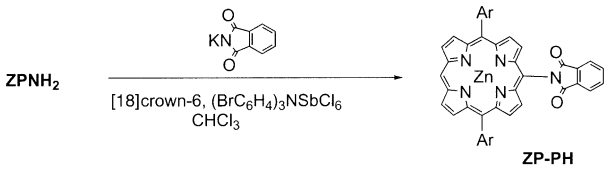

Scheme 5.

reaction with potassium 4-methylphthalimide but the yield of **ZP-Cl$_4$PH** was quite small, probably owing to the low solubility of potassium 3,4,5,6-tetrachlorophthalimide. A high concentration of a phthalimide anion is essential because of serious competition with the porphyrin *meso*–*meso* coupling reaction.[17] This direct introduction of the imide group is apparently more convenient than the stepwise method, but the low solubility of potassium phthalimides in $CHCl_3$ limits the range of this reaction.

Structures: Structural optimization of **ZP-Im** compounds has been carried out by the PM3 method (WinMOPAC 3.0) for a porphine substrate without 3,5-di-*tert*-butylphenyl groups. In the most stable conformation, a porphine and an imide are held in an approximately perpendicular geometry (88–91°). Both the porphine and imide rings are calculated to be quite planar and the center-to-center distances are calculated to be 8.49 Å in **ZP-NI**, 8.33 Å in **ZP-PI**, 7.90 Å in **ZP-NPH**, and 7.00 Å in the other dyads. The edge-to-edge distances (the bond length between the *meso*-carbon and the imide nitrogen) are calculated to be 1.43 Å in **ZP-NI**, 1.45 Å in **ZP-NPH**, and 1.41 Å in the other dyads. Calculation has also predicted that the thermal fluctuation of the dihedral angle is restricted within $90 \pm 15°$. The ^{1}H NMR spectra of **ZP-Im** display the porphyrin peripheral protons at nearly the same chemical shifts as those of Zn^{II} 5,10,15-tris(3,5-di-*tert*-butylphenyl)porphyrin (**ZTP**), indicating that the *meso*-substituted imide moiety in all **ZP-Im** takes on a nearly perpendicular conformation towards the porphyrin plane, similar to the *meso*-phenyl group in **ZTP**.

The X-ray structures of **ZP-PH**, **ZP-MPH**, **ZP-Cl$_2$PH**, and **ZP-Cl$_4$PH** were determined. The structure of **ZP-PH** is shown in Figure 1 and selected structural parameters are

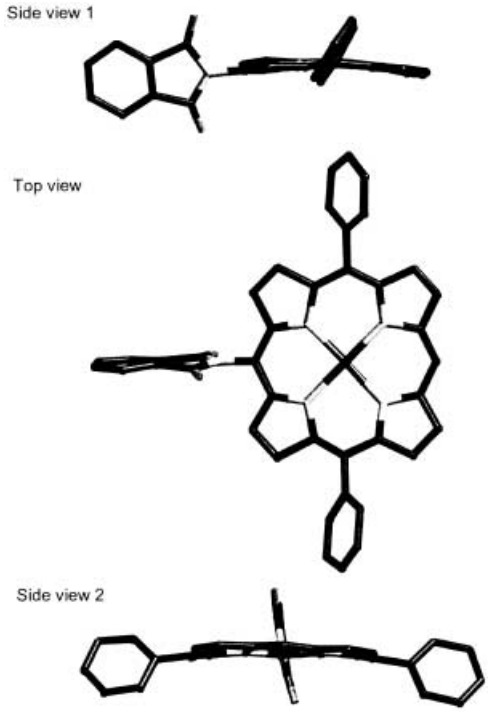

Figure 1. X-ray structure of **ZP-PH**. Hydrogen atoms and *tert*-butyl groups are omitted for clarity.

listed in Tables 1 and 2. In all of these cases, the imide moiety is rather planar but the porphyrin ring has a slightly ruffled conformation with relatively large mean plane deviations (0.55 Å **ZP-PH**, 0.57 Å **ZP-MPH**, 0.54 Å for **ZP-Cl$_2$PH**, and 0.48 Å **ZP-Cl$_4$PH**). The dihedral angles between the porphyrin and the imide are 76–88° and the center-to-center distances are 7.21–7.27 Å in **ZP-Cl$_2$PH** and 7.27 Å in **ZP-PH** with the edge-to-edge distances of 1.42–1.44 Å. These structural features are roughly consistent with those estimated by PM3 calculations. Although there are some differences in the geometrical parameters in the solid state, we may consider

Table 1. Data for X-ray structures of **ZP-Cl$_4$PH**, **ZP-Cl$_2$PH**, **ZP-PH**, and **H$_2$P-MPH**.

Compound	α[a] [Å]	β[b] [Å]	ϕ_1[c] [Å]	ϕ_2[d] [Å]	θ[e] [°]
ZP-Cl$_4$PH	1.437	7.21	0.480	0.040	80
ZP-Cl$_2$PH	1.435	7.22	0.574	0.020	76
ZP-PH	1.432	7.27	0.554	0.001	88
ZP-MPH	1.424	7.23	0.568	0.011	79

[a] α is the bond distance between the porphyrin *meso*-carbon and the imide nitrogen. [b] β is the center-to-center distance. [c] ϕ_1 is the porphyrin mean plane deviation. [d] ϕ_2 is the imide mean plane deviation. [e] θ is the dihedral angle.

Table 2. Crystal data and structure refinements for **ZP-Cl$_4$PH**, **ZP-Cl$_2$PH**, **ZP-PH**, and **ZP-MPH**.

	ZP-Cl$_4$PH	**ZP-Cl$_2$PH**	**ZP-PH**	**ZP-MPH**
formula	$C_{56}H_{51}Cl_4N_5O_2Zn$	$C_{56}H_{53}Cl_2N_5O_2Zn$	$C_{56}H_{55}N_5O_2Zn$	$C_{57}H_{57}N_5O_2Zn$
formula wt	1033.24	964.35	895.46	909.49
T [K]	123	123	123	123
λ [Å]	0.7107	0.7107	0.7107	0.7107
cryst system	triclinic	triclinic	triclinic	triclinic
space group	$P\bar{1}$	$P\bar{1}$	$P\bar{1}$	$P\bar{1}$
unit cell dimensions				
a [Å]	12.935(1)	14.2032(5)	14.0839(8)	14.1429(7)
b [Å]	13.627(1)	15.4030(7)	15.3743(8)	15.3850(9)
c [Å]	16.313(2)	15.5722(5)	15.548(1)	15.572(1)
α [°]	100.608(2)	109.353(3)	105.311(5)	109.046(3)
β [°]	100.273(3)	110.942(2)	112.791(2)	111.371(2)
γ [°]	95.921(3)	103.832(2)	101.076	103.733(2)
V [Å^3]	2753.5(4)	2743.7(2)	2824.7(4)	2727.2(3)
Z	2	2	2	2
ρ_{calcd} [g cm^{-3}]	1.387	1.167	1.053	1.107
μ [cm^{-1}]	7.860	5.872	4.75	4.925
$F(000)$	1192.00	1008.00	944.00	960.00
cryst size [mm^3]	0.40 × 0.40 × 0.10	0.40 × 0.40 × 0.20	0.60 × 0.40 × 0.20	0.20 × 0.20 × 0.10
$2\theta_{max}$ [°]	55.0	55.0	55.0	55.0
obsd reflctns	12286	12218	9997	11920
total reflctns	24459	24345	24376	21945
completeness to $\theta = 55.0°$ [%]	100.0	100.0	100.0	100.0
absorpn corrn	empirical	empirical	empirical	empirical
data/restraints/params	12286/0/715	12218/0/619	9997/0/640	11920/0/677
goodness of fit on F^2	0.785	1.170	3.520	0.840
final R indices R_1	0.045	0.083	0.081	0.080
$[I > 3\sigma(I)]$ wR_1	0.060	0.100	0.113	0.115
largest diff peak and hole [e Å^{-3}]	0.54/ – 0.45	1.81/ – 0.83	3.81/ – 0.92	1.27/ – 0.61

that the ET reaction in the **ZP-Im** models proceeds in a similar perpendicular conformation, which disrupts π-conjugation between the porphyrin and the imide.

Redox potentials: The first oxidation and reduction potentials versus the ferrocene/ferrocenium potential were measured in DMF by the differential pulse voltammetry method (Table 3). The first oxidation potentials (E_{ox}), which correspond to the one-electron oxidation of a Zn^{II} porphyrin donor, were in the 0.43 – 0.49 V range; this indicates that the effects of an attached imide group are not so significant. The first reduction potentials (E_{red}), which correspond to one-electron reduction of an imide acceptor, are in the -0.89 (**NI**) to ~ -1.69 V (**MPH**) range, reflecting the electron-accepting abilities of the respective imides. The correlation between E_{ox} and E_{red} is relatively weak, again indicating that the electronic interactions in the ground state are weak in **ZP-Im**. With eight **ZP-Im** dyads in hand, a wide range of $E_{ox} - E_{red}$ (1.32 – 2.15 V) and hence a wide range energy gaps associated with ET are now available for investigation of the energy-gap dependence on the CS.

Table 3. Redox potentails in DMF (vs ferrocene/ferrocenium; in V).

Compound	E_{ox}	E_{red}	$E_{ox} - E_{red}$
ZP-NI	0.43	– 0.89	1.32
ZP-NPH	0.48	– 1.08	1.56
ZP-PI	0.45	– 1.14	1.59
ZP-Cl$_4$PH	0.49	– 1.35	1.84
ZP-Cl$_2$PH	0.48	– 1.56	2.04
ZP-ClPH	0.44	– 1.64	2.08
ZP-PH	0.45	– 1.69	2.14
ZP-MPH	0.46	– 1.69	2.15

Steady-state spectroscopy: The UV/Vis absorption spectra are shown in Figure 2 and the numerical data are summarized in Table 4. All the **ZP-Im** dyads have almost the same absorption spectrum as that of **ZTP**, in which the Soret band is observed at 420 nm and the Q bands are observed at 551 and 589 nm in THF. Charge transfer absorption bands, which are clearly detected in *directly* linked porphyrin-quinone systems,[14, 15] are not detected in **ZP-Im**, suggesting weaker electronic interactions between **ZP** and **Im** in the ground state.

The fluorescence spectra of **ZP-Im**, taken for excitation at 546 nm in THF, are shown in Figure 3. The fluorescence spectral shapes remain nearly the same throughout the series, while the intensity decreases with an increase in the electron accepting ability of the imide moiety, reaching virtually no detectable fluorescence for **ZP-NI**, **ZP-NPH**, and **ZP-PI**. The fluorescence quantum yields, Φ_F, were determined with respect to the reported value of Zn^{II} TPP in benzene ($\Phi_F = 0.03$),[18] and are listed in Table 4. From these fluorescence quantum yields, the charge separation rates between ^{1}**ZP*** and **Im**, k_{CS}, were estimated by Equation (2), in which Φ_F^0 and Φ_F are the fluorescence quantum yields of reference porphyrin **ZTP** and **ZP-Im**, respectively, and τ^0 is the fluorescence lifetime of **ZTP**. The k_{CS} values obtained are listed in Table 5. The k_{CS} values estimated from the fluorescence quantum yield

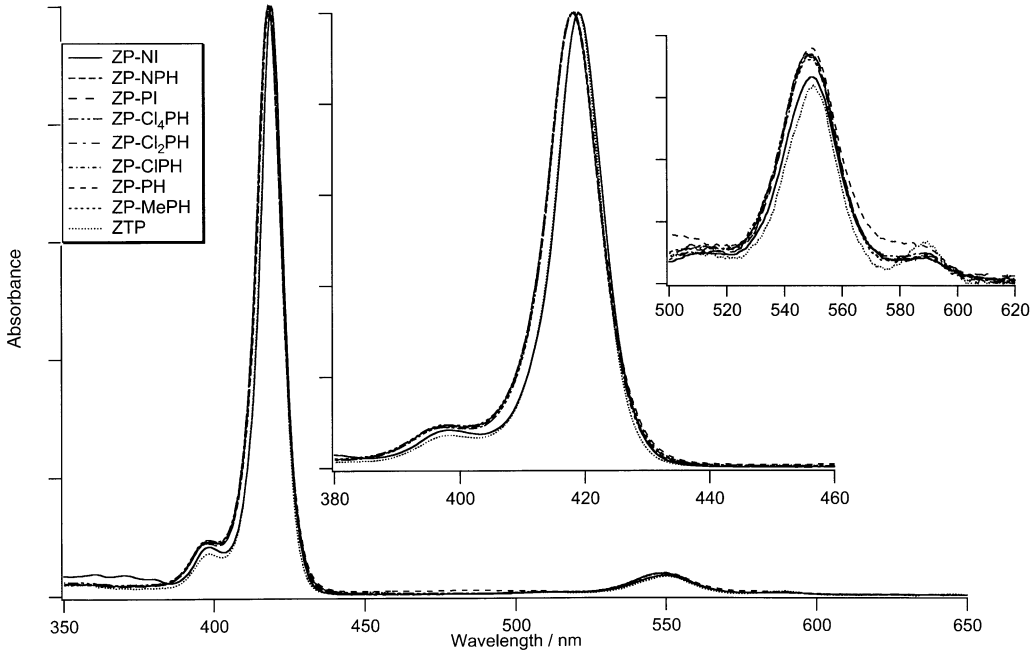

Figure 2. Absorption spectra of **ZTP** and **ZP-Im** in THF.

Table 4. Absorption and fluorescence spectra.

Compound	Toluene		THF		DMF	
	absorption	fluorescence [ϕ_F]	absorption	fluorescence [ϕ_F]	absorption	fluorescence [ϕ_F]
$ZnAr_3P$	419, 544, 583	590, 638 (0.028)	420, 551, 589	594, 644 (0.031)	422, 555, 593	597, 650 (0.046)
ZP-NI	421, 546, 579[a]	nd[b]	419, 550, 589	nd	421, 552, 591	nd
ZP-NPH	420, 545, 576[a]	nd	419, 550, 590	nd	421, 552, 593	nd
ZP-PI	420, 545, 576[a]	nd	419, 549, 589	nd	421, 552, 591	nd
ZP-Cl_4PH	420, 546, 576[a]	590, 637 (0.0012)	419, 549, 590	593, 650 (0.0012)	421, 551, 594	593, 650 (0.0012)
ZP-Cl_2PH	420, 545, 576[a]	590, 640 (0.024)	419, 550, 590	593, 647 (0.0030)	421, 552, 592	593, 650 (0.0009)
ZP-ClPH	420, 545, 576[a]	588, 640 (0.023)	419, 549, 589	593, 645 (0.018)	421, 552, 591	594, 651 (0.0030)
ZP-PH	420, 546, 576[a]	591, 638 (0.021)	419, 550, 589	593, 645 (0.021)	421, 553, 593	595, 649 (0.024)
ZP-MPH	420, 545, 576[a]	590, 639 (0.023)	419, 549, 589	593, 646 (0.022)	421, 552, 591	595, 649 (0.032)

[a] Shoulder; [b] not detected.

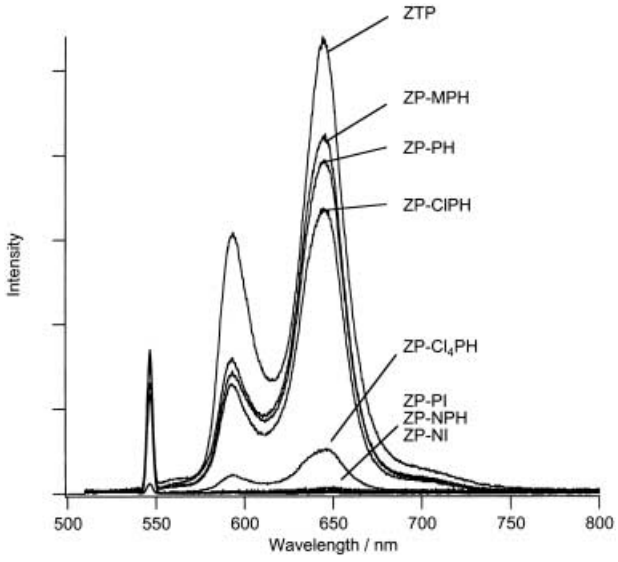

Figure 3. Fluorescence spectra of **ZTP** and **ZP-Im** taken for excitation at 546 nm in THF.

are less reliable in comparison to those based on the transient absorption data (discussed later), often owing to contamination by other fluorescent material. They do, however, provide a supplementary guide for estimating k_{CS} values that are not so large, for instance, in the cases of **ZP-MPH**, **ZP-PH**, and **ZP-ClPH**.

$$k_{CS} = \left(\frac{\Phi_F^0}{\Phi_F} - 1\right)(\tau^0)^{-1} \quad (2)$$

Transient absorption spectra: In order to confirm the ET events, we examined the transient absorption spectra of **ZP-Im**. We used two laser systems, a picosecond pump-probe system with 15 ps excitation pulse at 532 nm,[19] and a subpicosecond pump-probe system with a 160 fs tunable pulse.[20] Figure 4 shows the transient absorption spectra of **ZTP** in toluene at 20 ps and 6 ns delay times, which correspond to $S_1 \rightarrow S_n$ and $T_1 \rightarrow T_n$ absorptions, respectively. The $S_1 \rightarrow S_n$ absorption spectrum exhibits a peak at 460 nm and bleaching at 545, 590, and 645 nm. The bleaching at 545 and 590 nm corresponds to the ground-state absorption of

Table 5. Time constants of charge separation and recombination (k_{CS} and k_{CR} [s^{-1}]).

Compound	Toluene		THF		DMF	
	k_{CS}	k_{CR}	k_{CS}	k_{CR}	k_{CS}	k_{CR}
ZP-NI	1.1×10^{11}[a]	1.5×10^{10}[a]	7.7×10^{11}[a]	2.1×10^{11}[a]	2.0×10^{12}[a]	4.8×10^{11}[a]
ZP-NPH	1.9×10^{11}[a]	2.0×10^{10}[a]	5.3×10^{11}[a]	2.2×10^{11}[a]	1.0×10^{12}[a]	4.5×10^{11}[a]
ZP-PI	1.7×10^{11}[a]	1.1×10^{10}[a]	3.8×10^{11}[a]	1.1×10^{11}[a]	5.6×10^{11}[a]	3.2×10^{11}[a]
ZP-Cl_4PH	5.3×10^{10}[a]	3.6×10^{9}[a]	1.3×10^{11}[a]	4.5×10^{10}[a]	2.5×10^{11}[a]	1.1×10^{11}[a]
	9.5×10^{9}[b]		9.9×10^{9}[b]		1.4×10^{10}[b]	
ZP-Cl_2PH	7.6×10^{7}[b]		5.0×10^{10}[a]	4.0×10^{9}[a]	9.6×10^{10}[a]	1.6×10^{10}[a]
			3.6×10^{9}[b]		1.9×10^{9}[b]	
ZP-ClPH	1.0×10^{8}[b]		2.9×10^{8}[b]		8.0×10^{10}[a]	5.0×10^{9}[a]
					5.6×10^{9}[b]	
ZP-PH	1.4×10^{8}[b]		2.0×10^{8}[b]		3.5×10^{8}[b]	
ZP-MPH	9.9×10^{7}[b]		1.5×10^{8}[b]		1.7×10^{8}[b]	

[a] From fs transient absorption [b] From steady-state fluorescence quenching.

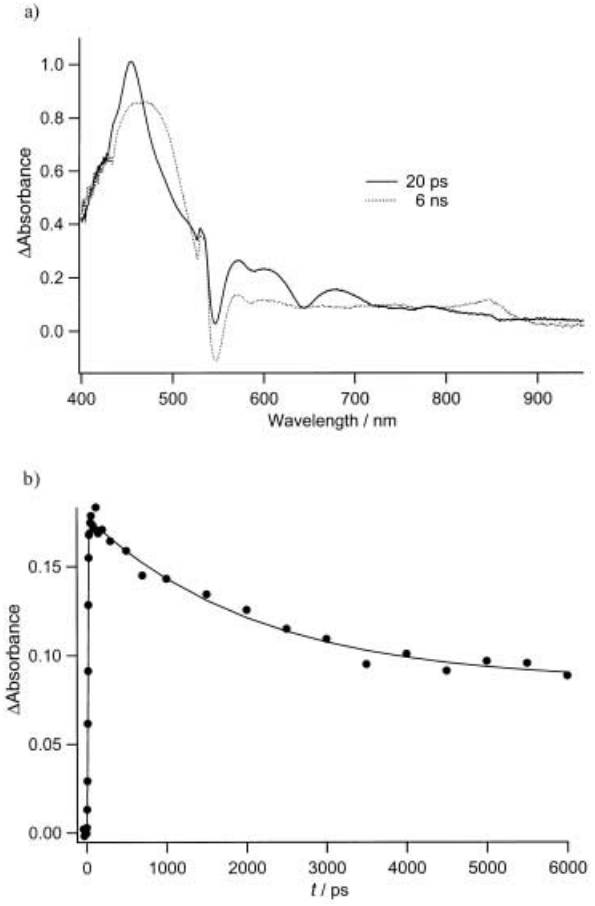

Figure 4. a) Transient absorption spectra of **ZTP** at 20 ps (solid line) and 6 ns delay times (dotted line) taken for excitation by a 532 nm laser pulse with 15 ps pulsewidth in toluene. b) Temporary profile of **ZTP** at 680 nm.

ZTP and that at 645 nm corresponds to the induced emission of ^{1}**ZTP***. The $T_1 \rightarrow T_n$ absorption spectrum shows broad bands around 490 and 850 nm and bleaching at 545 and 585 nm. Spectral evolutions from ^{1}**ZTP*** to ^{3}**ZTP*** were examined at 490, 600, 680, and 850 nm, commonly yielding time constants of 2.1 – 2.2 ns, in agreement with the fluorescence lifetime of **ZTP** (1.9 ns).

The transient absorption spectrum of **ZP-PI** in toluene exhibits a characteristic sharp absorption band at 705 nm due to **PI**$^-$ and an absorption band around 680 nm due to **ZP**$^+$ (Figure 5c), clearly providing evidence for CS. Bleaching at 545 nm is also consistent with the occurrence of CS, indicating depletion of the **ZP** ground state. The absorbance at 700 nm increases with $\tau \approx 5.8$ ps and decays with $\tau \approx 95$ ps (Figure 6c). The absorbance at 680 nm, due to **ZP**$^+$, exhibits essentially the same time-dependent profile as that at 700 nm. From the analysis of these time dependent profiles, the charge separation (k_{CS}) and charge recombination (k_{CR}) rates for **ZP-PI** were determined to be 1.7×10^{11} s^{-1} and 1.0×10^{10} s^{-1}, respectively. The transient absorption spectrum of **ZP-NI** exhibits, in addition to a broad band at 680 nm due to **ZP**$^+$, characteristic bands at 610, 670, and 790 nm (Figure 5a), which can be assigned to **NI**$^-$ on the basis of previous studies.[9] By following the same analysis, the rate constants

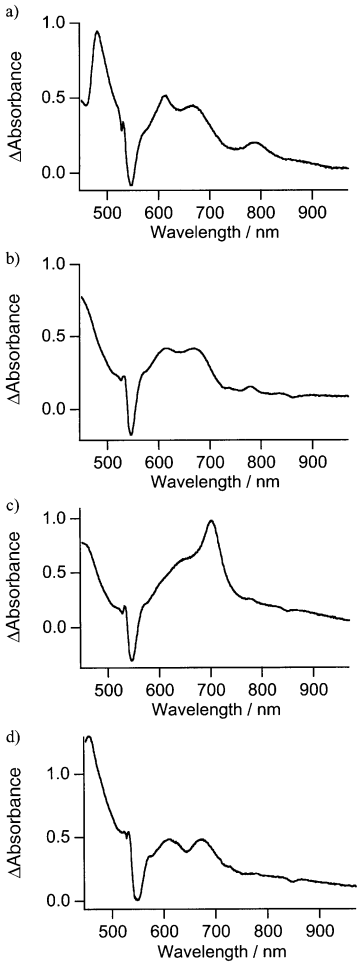

Figure 5. Transient absorption spectra at 20 ps delay time; a) **ZP-NI**, b) **ZP-NPH**, c) **ZP-PI**, and d) **ZP-Cl_4PH** taken for excitation at 532 nm in toluene.

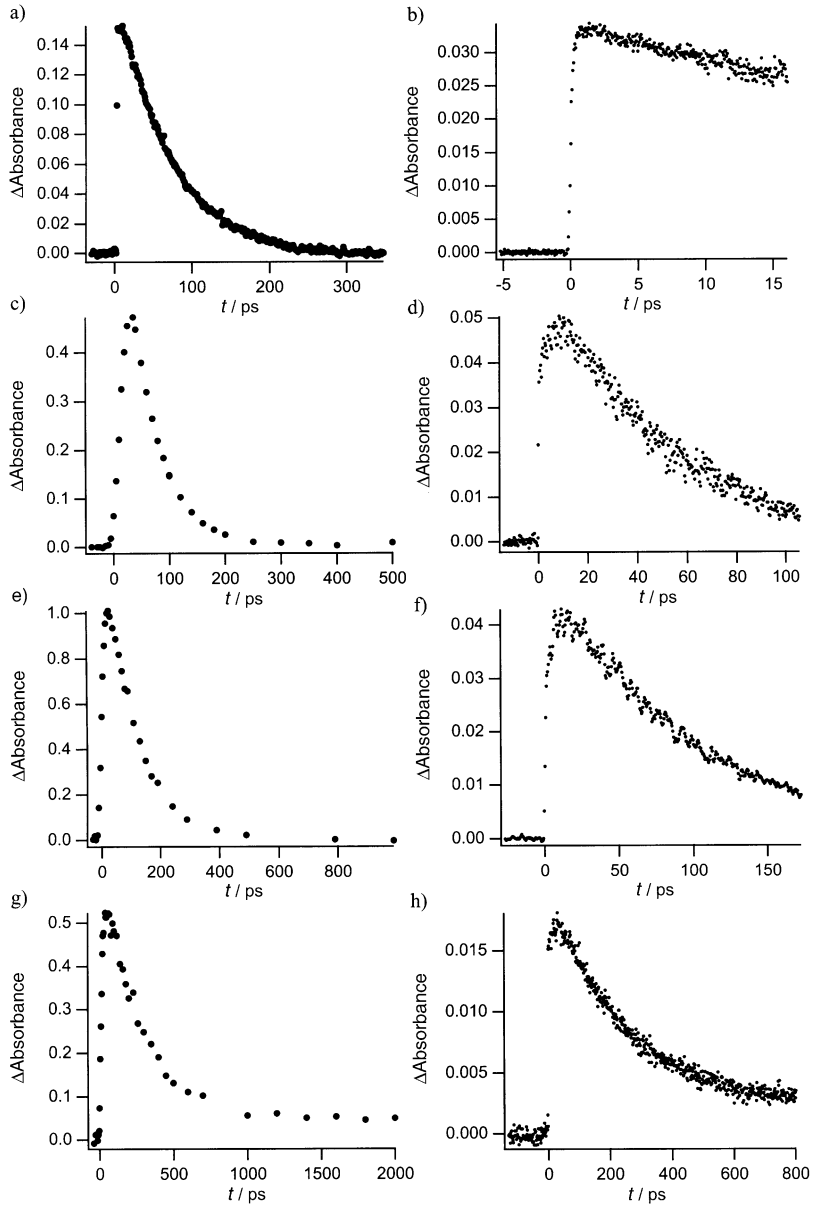

Figure 6. Temporary profiles of the transient absorption spectra in a) toluene; b) **ZP-NI** ($\lambda_{ex}=550$ nm, $\lambda_{pr}=700$ nm); c) **ZP-NPH** ($\lambda_{ex}=532$ nm, $\lambda_{pr}=680$ nm); d) **ZP-NPH** ($\lambda_{ex}=550$ nm, $\lambda_{pr}=680$ nm); e) **ZP-PI** ($\lambda_{ex}=532$ nm, $\lambda_{pr}=700$ nm); f) **ZP-PI** ($\lambda_{ex}=550$ nm, $\lambda_{pr}=700$ nm); g) **ZP-Cl$_4$PH** ($\lambda_{ex}=532$ nm, $\lambda_{pr}=680$ nm); and h) **ZP-Cl$_4$PH** ($\lambda_{ex}=550$ nm, $\lambda_{pr}=680$ nm) in toluene.

were determined; $k_{CS}=1.9\times10^{11}$ s^{-1} and $k_{CR}=2.0\times10^{10}$ s^{-1} for **ZP-NI**. The transient absorption spectra of both **ZP-NPH** and **ZP-Cl$_4$PH** displayed broad bands around 680 nm due to **ZP**$^+$, while the absorption bands due to **NPH**$^-$ and **Cl$_4$PH**$^-$ were not so prominent (Figure 5b and d). We have therefore monitored the time profiles at 680 nm (Figure 6b and d), from which we have determined k_{CS} and k_{CR} for **ZP-NPH** and **ZN-Cl$_4$PH** (Table 5). In toluene, **ZP-PH** and **ZP-MPH** had spectra and decay profiles almost identical to those of **ZnAr$_3$P**, and thus we concluded no CS in these dyads.

In THF, the transient absorption spectra confirmed the occurrence of CS for **ZP-NI**, **ZP-NPH**, **ZP-PI**, **ZP-Cl$_4$PH**, and **ZP-Cl$_2$PH**, while those of **ZP-MPH**, **ZP-PH**, and **ZP-ClPH** were the same as that of **ZnAr$_3$P** indicating that there was no CS. In more polar DMF, only **ZP-PH** and **ZP-MPH** did not exhibit CS. The k_{CS} and k_{CR} values are listed in Table 5. These values are roughly in agreement with those estimated from the steady-state fluorescence quenching.

Estimation of energy gaps in electron-transfer reactions: Energy gaps for the CS between ^{1}**ZP*** and **Im**, ΔG_{CS}, and of the CR in **ZP**$^+$**–Im**$^-$ ion pair, ΔG_{CR}, were estimated by Equations (3) and (4), in which $E(S_1)$ is the excitation energy to ^{1}**ZP***, ΔG_s is the correction term which includes the effects of solvent polarity and Coulombic interaction between the charged donor and acceptor. The correction term ΔG_s may be calculated by the Born equation [Eq. (5)],[21] but this treatment would often overstimate ΔG_s in low dipolar solvents.

$$-\Delta G_{CS}=E(S_1)+\Delta G_{CR} \quad (3)$$

$$-\Delta G_{CR}=E_{ox}-E_{red}+\Delta G_S \quad (4)$$

$$\Delta G_S=e^2\left(\frac{1}{2r_D}+\frac{1}{2r_A}\right)\left(\frac{1}{\varepsilon_s}-\frac{1}{\varepsilon_r}\right)-\frac{e^2}{\varepsilon_s r} \quad (5)$$

Alternatively, the correction term ΔG_s can be estimated when appropriate dyads **ZP-Im**, in which $E(S_1)$ is close to that of $-\Delta G_{CR}$ and thus $-\Delta G_{CS}$ is almost zero and its fluorescence exhibits biphasic decay, are available. Fortunately, we have observed such biphasic decays for **ZP-ClPH** and **ZP-Cl$_2$PH** in toluene (Figure 7), **ZP-PH** and **ZP-ClPH** in THF, and **ZP-PH** in DMF. In these cases, the fluorescence decays were fit with biexponential functions; 180 ps (23%) and 1620 ps (77%) for **ZP-ClPH** in toluene; 450 ps (21%) and 1500 ps (79%) for **ZP-Cl$_2$PH** in toluene; 280 ps (67%) and 1440 ps (33%) for **ZP-PH** in THF; 280 ps (58%) and 1190 ps (42%) for **ZP-ClPH** in THF; 160 ps (46%) and 1180 (54%) for **ZP-PH** in DMF. These biphasic decays were interpreted in terms of the thermal repopulation of the ion-pair state **ZP**$^+$**–Im**$^-$ to ^{1}**ZP***–**Im**, which has been well demonstrated for covalently linked donor-acceptor models with nearly zero $-\Delta G_{CS}$.[3c, 4, 5, 22]

Assuming the thermal repopulation of ^{1}**ZP***–**Im** from **ZP**$^+$**–Im**$^-$, k_{CS}, k_{-CS}, and k_{CR} were calculated according to well-established procedures [Eq. (6)–(10)], in which k_{-CS} is the rate of reverse electron transfer to generate ^{1}**ZP***–**Im**, k_0

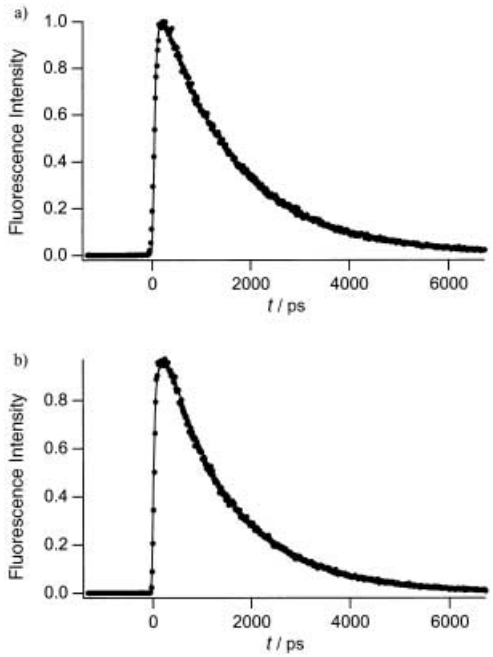

Figure 7. Fluorescence decay in toluene ($\lambda_{ex} = 590$ nm, $\lambda_{em} = 650$ nm); solid lines indicate biexponential fits as described in the text. a) **ZP-ClPH**; b) **ZP-Cl$_2$PH**.

is (1.9 ns)$^{-1}$ (the fluorescence lifetime of **ZTP**, 1.9 ns), and C_1, C_2, α, and β are the experimental values determined from the fluorescence decay analysis.

$$[^1\mathbf{ZP^*-Im}] = C_1 e^{-\alpha t} + C_2 e^{-\beta t} \quad (6)$$

$$\alpha = \tfrac{1}{2}\left(k_{CS} + k_{-CS} + k_0 + k_{CR} + \sqrt{(-k_{CS} + k_{-CS} - + k_0 + k_{CR})^2 + 4k_{CS}k_{-CS}}\right) \quad (7)$$

$$\beta = \tfrac{1}{2}\left(k_{CS} + k_{-CS} + k_0 + k_{CR} - \sqrt{(-k_{CS} + k_{-CS} - k_0 + k_{CR})^2 + 4k_{CS}k_{-CS}}\right) \quad (8)$$

$$C_1 = \frac{k_0 + k_{CS} - \beta}{\alpha - \beta} \quad (9)$$

$$C_2 = \frac{\alpha - k_0 - k_{CS}}{\alpha - \beta} \quad (10)$$

Through this analysis we calculated the values of k_{CS}, k_{-CS}, and k_{CR}. Based on the relation $-\Delta G_{CS} = RT\ln(k_{CS}/k_{-CS})$, in which $-\Delta G_{CS}$ is the energy gap for CS (^{1}**ZP*** **– Im** → **ZP$^+$ – Im$^-$**), the energy levels of **ZP$^+$ – Im$^-$** were estimated with respect to that of ^{1}**ZP* – Im**. These results are quite informative, allowing a direct estimate of the correction term, ΔG_s, in each solvent. The energy levels of the excited states E(S_1) were determined on the basis of the absorption (0,0) and corresponding fluorescence (0,0) bands; 2.115 eV in toluene, 2.097 eV in THF, and 2.084 eV in DMF. The results obtained for **ZP-ClPH** and **ZP-Cl$_2$PH** in toluene led to placement of the ion-pair state **ZP$^+$ – Im$^-$** above the ^{1}**ZP*** state by 0.027 and 0.015 eV, respectively, which in turn allowed us to estimate ΔG_s in Equation (4) to be 0.062 and 0.090 eV. Thus, we used an average value of 0.076 eV for ΔG_s in toluene. Similarly, from the results for **ZP-PH** and **ZP-ClPH** in THF we estimated an average value of -0.03 eV for ΔG_s. The results for **ZP-PH** in DMF led to a correction term of -0.06 eV. Energy-gap values thus estimated indicate that there is a wide range of energy gaps available; $-\Delta G_{CS}$ and $-\Delta G_{CR}$ respectively cover a range of -0.06 – 0.77 eV and 1.32 – 2.15 eV in DMF, of -0.09 – 0.74 eV and 1.36 – 2.19 eV in THF, and of -0.20 – 0.64 eV and 1.47 – 2.32 eV in toluene (Table 6).

Table 6. Energy gaps of charge separation ($-\Delta G_{CS}$) and recombination ($-\Delta G_{CR}$).[a]

Compound	$-\Delta G_{CS}$			$-\Delta G_{CR}$		
	toluene	THF	DMF	toluene	THF	DMF
ZP-NI	0.71	0.81	0.82	1.41	1.29	1.26
ZP-NPH	0.48	0.57	0.58	1.64	1.53	1.50
ZP-PI	0.46	0.54	0.55	1.66	1.56	1.53
ZP-Cl$_4$PH	0.20	0.29	0.30	1.92	1.81	1.78
ZP-Cl$_2$PH	-0.01	0.09	0.10	2.12	2.01	1.97
ZP-ClPH	-0.045	0.05	0.06	2.16	2.05	2.02
ZP-PH	-0.11	-0.01	0.00	2.22	2.11	2.08
ZP-MPH	-0.13	-0.02	-0.01	2.24	2.12	2.09

[a] The energy levels of the excited states $E(S_1)$ were determined on the basis of the corresponding fluorescence and absorption (0,0) bands; 2.115 eV in toluene, 2.097 eV in THF, and 2.084 eV in DMF. The correction terms ΔG_S of Equation (4) have been estimated on the basis of the biexponential fluorescence decays of **ZP-ClPH** and **ZP-Cl$_2$PH** in toluene and **ZP-PH** and **ZP-ClPH** in THF, and **ZP-PH** in DMF. We used averaged values of 0.076 eV in toluene and -0.03 eV in THF, and a value of -0.06 eV in DMF.

Energy-gap dependence of k_{CS} and k_{CR} in the framework of nonadiabatic ET reaction: The ET reaction rate constants obtained in toluene, THF, and DMF solutions were analyzed on the basis of the nonadiabatic electron transfer theory, in which it is assumed that the intrachromophore high-frequency vibrations can be replaced by one mode with an averaged frequency, and the solvent can be treated as a dielectric continuum. The well-known expression in the above framework is given in Equations (11) – (13).[1b]

$$k_{ET} = \sqrt{\frac{\pi}{\hbar^2 \lambda_S k_B T}}\,|V|^2 \sum_0^\infty \left(\frac{e^{-S}S^n}{n!}\right) \exp\{-\frac{(\lambda_S + \Delta G + n\hbar\langle\omega\rangle^2)}{4\lambda_S k_B T}\} \quad (11)$$

$$S = \frac{\lambda_V}{\hbar\langle\omega\rangle} \quad (12)$$

$$\lambda_S = e^2\left(\frac{1}{2r_A} + \frac{1}{2r_D} - \frac{1}{R}\right)\left(\frac{1}{n^2} - \frac{1}{\varepsilon}\right) \quad (13)$$

In these equations, $S = \lambda_v/\hbar\langle\omega\rangle$ is the electron-vibration coupling constant; λ_v is the reorganization energy associated with the averaged angular frequency $\langle\omega\rangle$, and λ_s is the solvent reorganization energy.

Figure 8 shows semilogarithmic plots of k_{CS} and k_{CR} against $|\Delta G_{CS}|$ and $|\Delta G_{CR}|$ for **ZP-Im** studied here and their simulations by means of Equation (11) in toluene, THF, and DMF. In each case we used a value of 1500 cm^{-1} for $\langle\omega\rangle$ on the basis of the porphyrin macrocycle C=C double-bond frequency. In addition, the λ_v value of 0.3 eV, which was obtained for the CS reaction in the S_2 state of the present systems,[10] was employed for all the analyses.

First we determined other key parameters from the best fit in the case of THF solution at $T = 295$ K. The result calculated with $\lambda_s = 0.64$ eV and $V = 14$ meV is shown as the solid line in Figure 8b. As mentioned in the introductory section, the

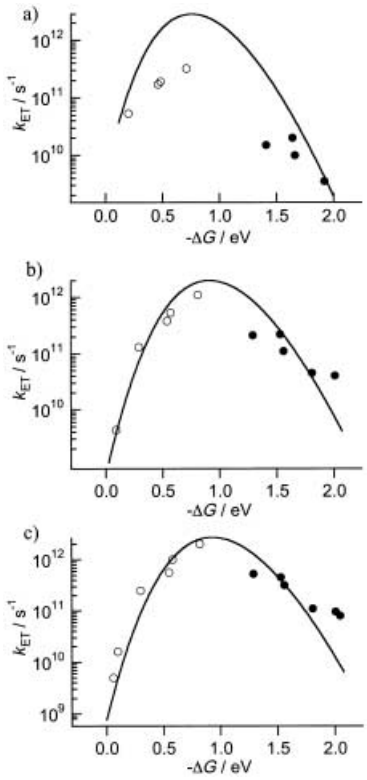

Figure 8. Energy gap dependence of k_{CS} (○) and k_{CR} (●) for ZP-Imide dyads in a) toluene, b) THF, and c) DMF. The curves were calculated by means of Equation (11), with common parameters $T = 295$ K, $\lambda_v = 0.3$ eV, $V = 14$ meV, $h\langle\omega\rangle = 0.15$ eV, and $\lambda_s = 0.46$ eV in toluene, 0.64 eV in THF, and 0.65 eV in DMF.

energy gap dependence of the CS process from the S_2 state was investigated in various solvents for the present **ZP-Im** systems[10] and the λ_s and V values in THF solutions were found to be 0.55 eV and 24 meV, respectively. Compared to these values for the CS process in the S_2 state, the present λ_s is slightly larger and the V value is smaller. These differences may be explained in the following manner. Firstly, the k_{CS} values in the S_2 state were on the order of $\geq 10^{12}$ s^{-1}, which is comparable to or faster than the solvent reorientation time of THF (ca. 0.5 ps).[23] In contrast, the present CS process in the S_1 state and the CR of the charge-separated state take place with a rate constant of $\leq 10^{12}$ s^{-1}, for which a solvent reorientation process can follow. Hence, the contribution from the solvent reorientational motion to the total solvent reorganization energy may become smaller for such a fast ET process in the S_2 state. Secondly, the smaller V value in the present ET processes indicates that the interchromophore electronic coupling for the charge separated species is larger in the S_2 state than in the S_1 state. Although it is difficult to derive a quantitative conclusion from this result, the rather widely spread MO in the S_2 state may lead to larger electronic coupling with the vacant MO of an acceptor.

The V value of 14 meV originating from ET processes in the present S_1 state is, however, still considerably large compared to those obtained for some other porphyrin systems, 3.8 meV for the porphyrin-1,4-phenylene-methylene-quinone bridged systems[4a] and about 6 meV for the porphyrin-quinone dyads linked by 1,4-phenylene-amide-1,4-phenylene spacer.[24] The large V value for the present systems might be accounted for by a short D – A distance through the direct connection. It is interesting to note that a V value of 9.4 meV was obtained for the ET dynamics in 1,4-phenylene-bridged zinc-free-base hybrid diporphyrins in which the D – A distance was larger than the present systems.[4a] In addition, comparison of the experimentally determined V values for the previously reported molecules with various spacers implies that not only the D – A distance but also the electronic properties of spacers play an important role in the ET dynamics; the use of a conjugated spacer leads to the enhancement of the tunneling matrix element for the ET process.[25]

The energy gap dependences of the ET rate constants in toluene and DMF were analyzed by adjusting only the λ_s value with other parameters fixed; the results with $\lambda_s = 0.46$ eV for toluene and $\lambda_s = 0.65$ eV for DMF are shown in Figures 8a and c. The deviation of the simulated curve from the experimental results for k_{CS} and k_{CR} is larger in toluene than in the two polar solvents. The simulated curve with the fixed parameter of $V =$ 14 meV for toluene suggests that this V value is overestimated. We will discuss this below.

The estimated λ_s value of 0.46 eV is much larger than that (ca. 0.01 eV) calculated by means of Equation (13). It is worth noting here that similarly large λ_s values were also observed for the porphyrin – quinone linked system[4a] and zinc-free-base porphyrin dyads,[5] for which λ_s values of 0.3 – 0.35 eV were estimated in benzene. Equation (13) was derived under the assumption that the simple linear response for the polarization of solvent is applicable in the solute – solvent interactions, and that the solvent can be regarded as the dielectric continuum. The present and previous results[4a, 5] indicate that the actual interactions between the solute and solvent in the ET processes may include some nonlinear solute – solvent interactions and discrete molecular structures within the solution. Recent theoretical treatments of the energetics of ET reactions in solution based on such molecular theories of solution structures seem to agree with the above experimental λ_s values.[26] Although the analysis based on Equation (12) suggests some unknown specific solute – solvent interactions, the simulation curve in Figure 8a, obtained by adjusting only λ_s to a smaller value, corresponds reasonably well to the energy-gap dependence, covering the whole energy-gap region including CS and CR.

Although a relatively large λ_s value was estimated by fitting the energy gap dependence of ET in nonpolar toluene solution, those in THF and DMF were estimated to be rather small and the difference between THF and DMF was intriguingly small. Similar results were also obtained in a previous study on the energy gap dependence in 1,4-phenylene-bridged zinc-free-base hybrid diporphyrin systems.[5] In contrast, a quite different solvent polarity dependence of λ_s was observed in the case of the porphyrin-quinone dyads with 1,4-phenylene-methylene spacer,[4a] for which λ_s increased more clearly with increasing solvent polarity. The present solvent polarity dependence of λ_s may arise because the positive and negative charges are held at a very short distance, giving rise to somewhat specific solvation of the ion-pair state, which may lead to weaker interactions with polar solvents.

Although the tunneling-matrix element of $V = 14$ meV is considerably large, it is possible to fit the observed ET rate constants, including both k_{CS} and k_{CR}, to the simulation calculated by means of Equation (11) over a wide energy-gap range, both in THF and DMF solutions. This presumably indicates that the nonadiabatic mechanism is still operative for the present **ZP-Im** system as a whole.

Energy-gap dependence of k_{CR} in the framework of radiationless transition: The simulations of the experimental results shown in Figure 8, which cover a wide energy-gap range, were not possible in the framework of the classical Marcus equation. This means that the contribution from the intrachromophore high-frequency vibrational modes for the ET in the inverted region is of crucial importance in this system. It should be noted that the nature of the ET in the so-called inverted region is fundamentally different from that in the normal region. As discussed in a previous paper,[5a] the CR in the inverted region is conceptually analogous to the radiationless transition (internal conversion) in the weak coupling limit, because of the embedded nature of the potential surface of the initial state in that of the final state and because of the transition between different eigenstates of the same Hamiltonian, which in turn is due to the coupling with promoting and accepting quantum modes of the intramolecular vibrations. Namely, the transition in the inverted region is greatly facilitated by the quantum-mechanical tunneling due to intrachromophore high-frequency modes. Such tunneling effects are not so important in the normal region, owing to the different nature of the energy surfaces. Moreover, such a quantum-tunneling mechanism may be more effective in systems with stronger interchromophore electronic interactions, such as compact ion pairs[7] and covalently linked systems with stronger interchromophore interactions as the porphyrin dyad systems.[5a]

On the basis of the theoretical treatments of the radiationless transition in the weak coupling limit,[27] an approximate relation for the energy-gap dependency of k_{CR} in the inverted region is given by Equations (14) and (15).

$$\ln k_{CR} = \ln C - \left(\frac{\gamma}{\hbar\omega_M}\right) |\Delta G_{CR}| \quad (14)$$

$$\gamma = \ln\left(\frac{|\Delta G_{CR}|}{\hbar\omega_M S_M}\right) - 1 \quad (15)$$

Here the pre-exponential factor C mainly represents the contribution from the electronic coupling term connecting the ion pair and the ground state and also some additional terms. The term $-(\gamma/\hbar\omega_M)\,|\Delta G_{CR}|$ arises from the energy release into the acceptor modes in the ion pair in the course of transition to the ground state. S_M and ω_M are average quantities for electron-vibrational coupling constants and angular frequencies of the quantum modes, respectively. Although γ contains ΔG_{CR}, its variation with the change of ΔG_{CR} is much smaller than the $|\Delta G_{CR}|$ itself in the term $-(\gamma/\hbar\omega_M)\,|\Delta G_{CR}|$.

Figure 9 shows the energy gap dependence of the CR rate constants in the present systems in three different solutions, and suggests that the relation $\ln k_{CR} = \alpha - \beta\,|\Delta G_{CR}|$ is applicable to the experimental results. The β values corresponding to $(\gamma/\hbar\omega_M)$ for these three solvents were almost identical to each other, whereas the α values were different; the α values for THF and DMF solutions were rather close while that in toluene as smaller. In an extreme case of such a supramolecule composed of very strongly interacting D and A, the main contribution to C may be the electronic matrix element of the kinetic energy parameter for the internal conversion between the excited state with large CT degree and the ground state with much smaller CT degree.[27–29] Namely, the two electronic states are mixed by coupling to promoting vibrations that break down the orthogonality of the Born – Oppenheimer states. In the previous section on the whole energy gap dependence as shown in Figure 8, we pointed out that the V value in toluene might be smaller than the fixed value of 14 meV. The analysis based on Equations (14) and (15) also suggests a similar tendency. This means that the electronic matrix element of the present large value of 14 meV obtained by Equation (11) includes the contribution from the mixing of the two electronic states by coupling to promoting vibrations that break down the orthogonality of these two states. The small α value in toluene suggests that the degree of mixing is small because of the low polarity of the solvent.

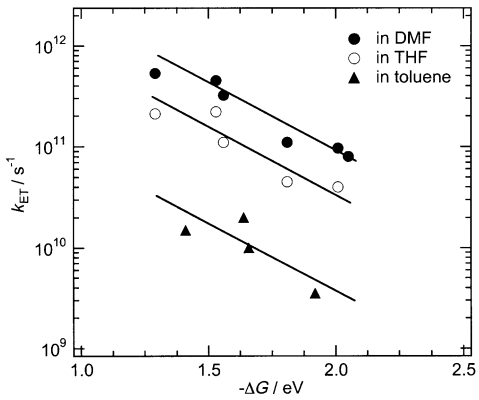

Figure 9. logk_{CR} versus $|\Delta G_{CR}|$ linear plots for toluene, THF, and DMF solutions.

In summarizing the above results and discussion, the following can be deduced: Although the tunneling-matrix element of $V = 14$ meV is considerably large, the fact that the simulations of the observed ET rate constants, including both k_{CS} and k_{CR}, calculated by means of Equation (11), seem to reproduce the experimental results in THF and DMF over a wide energy-gap range. This presumably indicates that the nonadiabatic mechanism is still operative. However, as shown in Figure 9, the energy-gap dependencies of k_{CR} could be reproduced as well or better by the linear energy-gap law, which was previously observed for the CR of CIPs (contact ion pairs) with strong inter-ionic interactions.[7]

Experimental Section

General: All reagents and solvents were of commercial reagent grade and were used without further purification except where noted. Dry CH_2Cl_2 was obtained by refluxing and distilling over P_2O_5. Dry $CHCl_3$ was

obtained by refluxing and distilling over CaH_2. Preparative separations were performed by silica gel flash column chromatography (Merck Kieselgel 60H No. 7736), silica gel gravity column chromatography (Wako gel C-200), and GPC column chromatography (BioRad, Bio-Beads SX-1). ^{1}H NMR spectra were recorded in $CDCl_3$ solution on a JEOL ALPHA-500 spectrometer (operating at 500 MHz), and chemical shifts were reported relative to the internal standard of $CHCl_3$ ($\delta = 7.260$) in ppm. UV/Vis absorption spectra were recorded on a Shimadzu UV-2400PC spectrometer. Steady-state fluorescence emission spectra were recorded on a Shimadzu RF-5300PC spectrometer. Mass spectra were recorded on a JEOL HX-110 spectrometer, using the positive-FAB ionization method with accelerating voltage 10 kV and a 3-nitrobenzylalcohol matrix. Redox potentials were measured by cyclic voltammetry or differential pulse voltammetry on a BAS electrochemical analyzer model 660.

Picosecond transient absorption spectra were measured by means of a microcomputer-controlled laser photolysis system with a custom-built repetitive mode-locked Nd^{3+}/YAG laser. The second harmonic of the Nd^{3+}/YAG laser at 532 nm with 15 ps fwhm was used for excitation. For detection with higher time resolution, a dual OPA femtosecond laser system was employed. The output of the Ti/sapphire oscillator (65 fs fwhm, 800 nm, 800 mW, 82 MHz) was regeneratively amplified. This amplified pulse (90 fs fwhm, 1 W, 1 kHz) was divided into two pulses with the same energy and guided into the OPA system. By using several nonlinear crystals, the OPA can cover the wavelength region from 300 nm to 3 μm with the output energy of a few to several tens of μJ per pulse. One of the two OPA systems was used for the pump light source and the other for the probe pulse. The output energy of the probe pulse was reduced to 1/1000. The pulse duration estimated by the cross-correlation between the pump and probe pulses at the sample position was 160 fs.

The fluorescence spectra were recorded by a scanning SLM-AMINCO 4800 spectrofluorometer, which makes it possible to obtain the corrected fluorescence spectra using Rhodamine B as a quantum counter. Picosecond time-resolved fluorescence experiments were carried out by using the time-correlated single photon counting (TCSPC) method.[30] The picosecond excitation pulses were obtained from a cavity-dumped picosecond dye laser (Coherent 702) synchronously pumped by a mode-locked Nd:YAG laser (Coherent Antares 76-s). The cavity-dumped beam from the dye laser has a 2 ps pulse width and an average power of about 40 mW at a 3.8 MHz dumping rate when Rhodamine 6G was used as the gain dye. The emission was collected at 45° with respect to the excitation laser beam by 5 and 25 cm focal length lenses, focused onto a monochromator (Jobin – Yvon HR320), and detected with a microchannel plate photomultiplier tube (Hamamatsu R2809U). The signal was amplified by a wideband amplifier (Philip Scientific), sent to a Quad constant fraction discriminator (Tennelec), a time-to-amplitude converter (Tennelec), a counter (Ortec), and a multi-channel analyzer (Tennelec/Nucleus), and stored on a computer.

Zn^{II} 5,15-Bis(3,5-di-*tert*-butylphenyl)-10-nitroporphyrin ZPNO$_2$: A solution of $AgNO_2$ (46 mg, 0.3 mmol) in MeCN (6 mL) was added to a solution of Zn^{II} 5,15-bis(3,5-di-*tert*-butylphenyl)porphyrin (**ZDP**; 225 mg, 0.30 mmol) and I_2 (38 mg, 0.15 mmol) in $CHCl_3$ (100 mL). After stirring for 1 h, the mixture was washed with water, aqueous $Na_2S_2O_3$, water, and brine, and was dried over anhydrous Na_2SO_4. The solvent was removed by rotary evaporator and the residue was separated by silica gel flash column chromatography with CH_2Cl_2/*n*-hexane 1:1 as eluent. A solution of $Zn(OAc)_2$ in methanol was added to a CH_2Cl_2 solution of the free-base porphyrin thus obtained. After stirring for 1 h, the solution was washed with water and brine and was dried over anhydrous Na_2SO_4. The solvent was removed by rotary evaporator to give **ZPNO$_2$** (235 mg, 98% yield). ^{1}H NMR ($CDCl_3$): $\delta = 10.35$ (s, 1H), 9.42 (d, $J = 5$ Hz, 2H), 9.40 (d, $J = 5$ Hz, 2H), 9.15 (d, $J = 5$ Hz, 2H), 9.11 (d, $J = 5$ Hz, 2H), 8.07 (d, $J = 2$ Hz, 4H), 7.86 (t, $J = 2$ Hz, 2H), 1.56 (s, 36H); UV (CH_2Cl_2): $\lambda_{max} = 417$, 546, 586 nm; fluorescence (CH_2Cl_2, $\lambda_{ex} = 417$ nm): $\lambda_{em} = 626$, 664 nm; FAB MS: calcd for $C_{56}H_{57}N_5O_2$: 793.3; found: 793 [M^+]; elemental analysis calcd (%) for $C_{48}H_{51}N_5O_2Zn$: C 72.49, H 6.46, N 8.81; found C 72.59, H 6.57, N 8.55.

Zn^{II} 10-Amino-5,15-bis(3,5-di-*tert*-butylphenyl)porphyrin ZPNH$_2$: Concentrated HCl (10 mL) was added slowly to a solution of **ZPNO$_2$** (235 mg, 0.30 mmol) and $SnCl_2$ (677 mg, 3.0 mmol) in dry diethyl ether (100 mL). After refluxing for 7 h, the mixture was carefully neutralized with concentrated aqueous NH_3, and the product was extracted with CH_2Cl_2, washed with water and brine, and dried over anhydrous Na_2SO_4. After the removal of the solvent with a rotary evaporator, the product was separated by silica gel column chromatography with CH_2Cl_2/hexane 1:1 as eluent. The free-base *meso*-amino substituted porphyrin (**H$_2$PNH$_2$**) thus obtained was dissolved in CH_2Cl_2 and was added to a solution of $Zn(OAc)_2$ in methanol. The resulting solution was stirred for 1 h, washed with water and brine, and dried over anhydrous Na_2SO_4. After the evaporation of the solvent, **ZPNH$_2$** was precipitated from a mixture of hexane and CH_2Cl_2 (183 mg, 87% yield). ^{1}H NMR ($CDCl_3$): $\delta = 9.35$ (s, 1H), 9.06 (d, $J = 5$ Hz, 2H), 8.87 (d, $J = 5$ Hz, 2H), 8.71 (d, $J = 5$ Hz, 2H), 8.61 (d, $J = 5$ Hz, 2H), 7.96 (d, $J = 2$ Hz, 4H), 7.73 (t, $J = 2$ Hz, 4H), 6.42 (br s, 2H), 1.51 (s, 36H); UV (THF): $\lambda_{max} = 428$, 541, 601, 646 nm; fluorescence (CH_2Cl_2, $\lambda_{ex} = 428$ nm): $\lambda_{em} = 660$, 713 nm; FAB MS: calcd for $C_{48}H_{55}N_5$: 763.4; found: 763 [M^+]; elemental analysis calcd (%) for $C_{48}H_{53}N_5Zn \cdot 2HCl$: C 68.77, H 6.61, N 8.35; found: C 68.46, H 6.39, N 8.10.

General procedure for synthesis of ZP-Im from ZPNH$_2$: A solution of **ZPNH$_2$** and anhydride (5 – 10 equiv) in pyridine or *N*,*N*-dimethylacetamide was heated under reflux for 5 h – 2 d. After evaporation of the solvent, CH_2Cl_2 was added to the reaction mixture and the resulting solution was filtered once. The **ZP-Im** product was separated over a silica gel column with CH_2Cl_2/*n*-hexane as eluent.

General procedure for synthesis of ZP-Im from ZDP: A solution of **ZDP**, potassium phthalimide derivatives (5 – 10 equiv), and [18]crown-6 in $CHCl_3$ was added to a solution of $(BrC_6H_4)_3NSbCl_6$ (1 equiv) in $CHCl_3$. After stirring for 1 – 2 h at room temperature, the solution was washed with water and brine, and was dried over anhydrous Na_2SO_4. After Zn^{II} ion insertion, the products were separated by GPC chromatography with toluene as eluent or silica gel flash column chromatography with CH_2Cl_2/hexane as eluent. Precipitation from CH_2Cl_2/*n*-hexane gave **ZP-Im**.

ZP-MPH: This compound was prepared in 38% yield by the condensation reaction of **ZPNH$_2$** with 4-methylphthalic anhydride. ^{1}H NMR ($CDCl_3$): $\delta = 10.32$ (s, 1H), 9.42 (d, $J = 5$ Hz, 2H), 9.14 (d, $J = 5$ Hz, 2H), 9.11 (d, $J = 5$ Hz, 2H), 9.09 (d, $J = 5$ Hz, 2H), 8.16 (d, $J = 7$ Hz, 1H), 8.10 (d, $J = 2$ Hz, 4H), 8.09 (s, 1H), 7.84 (d, $J = 7$ Hz, 1H), 7.83 (t, $J = 2$ Hz, 2H), 2.73 (s, 3H), 1.56 (s, 36H); UV (THF): $\lambda_{max} = 419$, 549, 589 nm; fluorescence (THF, $\lambda_{ex} = 546$ nm): $\lambda_{em} = 593$, 646 nm; FAB MS: calcd for $C_{57}H_{57}N_5O_2Zn$: 907.4; found: 907 [M^+]; elemental analysis calcd (%) for $C_{57}H_{57}N_5O_2Zn \cdot C_2H_5OH \cdot C_5H_5N \cdot H_2O$: C 73.02, H 6.70, N 7.92; found C 73.27, H 6.64 N 7.97.

ZP-PH: This compound was prepared in 41% yield by the condensation reaction of **ZPNH$_2$** with phthalic anhydride and in 35% yield by the direct introduction of phthalimide anion to **ZDP**. ^{1}H NMR ($CDCl_3$): $\delta = 10.34$ (s, 1H), 9.43 (d, $J = 5$ Hz, 2H), 9.15 (d, $J = 5$ Hz, 2H), 9.13 (d, $J = 5$ Hz, 2H), 9.10 (d, $J = 5$ Hz, 2H), 8.29 (dd, $J = 3$, 6 Hz, 2H), 8.10 (d, $J = 2$ Hz, 4H), 8.04 (dd, $J = 3$, 6 Hz, 2H), 7.82 (t, $J = 2$ Hz, 2H), 1.55 (s, 36H); UV (THF): $\lambda_{max} = 419$, 550, 589 nm; fluorescence (THF, $\lambda_{ex} = 546$ nm): $\lambda_{em} = 593$, 645 nm; FAB MS: calcd for $C_{56}H_{55}N_5O_2Zn$: 893.4; found: 893 [M^+]; elemental analysis calcd (%) for $C_{56}H_{55}N_5O_2Zn \cdot C_2H_5OH$: C 73.99, H 6.53, N 7.44; found C 74.08, H 6.26, N 7.60.

ZP-ClPH: This compound was prepared in 33% yield by the condensation reaction of **ZPNH$_2$** with 4-chlorophthalic anhydride. ^{1}H NMR ($CDCl_3$): $\delta = 10.33$ (s, 1H), 9.42 (d, $J = 5$ Hz, 2H), 9.13 (d, $J = 5$ Hz, 2H), 9.09 (d, $J = 5$ Hz, 2H), 9.08 (d, $J = 5$ Hz, 2H), 8.25 (d, $J = 2$ Hz, 1H), 8.22 (d, $J = 8$ Hz, 1H), 8.09 (d, $J = 2$ Hz, 4H), 8.02 (dd, $J = 2$, 8 Hz, 1H), 7.82 (t, $J = 2$ Hz, 2H), 1.55 (s, 36H); UV (THF): $\lambda_{max} = 419$, 549, 589 nm; fluorescence (THF, $\lambda_{ex} = 546$ nm): $\lambda_{em} = 593$, 645 nm; FAB MS: calcd for $C_{56}H_{54}ClN_5O_2Zn$: 927.3; found: 927 [M^+]; elemental analysis calcd (%) for $C_{56}H_{54}ClN_5O_2Zn \cdot C_2H_5OH$: C 71.38, H 6.20, N 7.18; found C 71.47, H 6.01, N 7.35.

ZP-Cl$_2$PH: This compound was prepared in 48% yield by the condensation reaction of **ZPNH$_2$** with 4,5-dichlorophthalic anhydride. ^{1}H NMR ($CDCl_3$): $\delta = 10.34$ (s, 1H), 9.43 (d, $J = 5$ Hz, 2H), 9.14 (d, $J = 5$ Hz, 2H), 9.11 (d, $J = 5$ Hz, 2H), 9.05 (d, $J = 5$ Hz, 2H), 8.36 (s, 2H), 8.09 (d, $J = 2$ Hz, 4H), 7.83 (t, $J = 2$ Hz, 2H), 7.83 (t, $J = 2$ Hz, 2H), 1.55 (s, 36H); UV (THF): $\lambda_{max} = 419$, 550, 590 nm; fluorescence (THF, $\lambda_{ex} = 546$ nm): $\lambda_{em} = 593$, 647 nm; FAB MS: calcd for $C_{56}H_{53}Cl_2N_5O_2Zn$: 961.3; found: 962 [M^+]; elemental analysis calcd (%) for $C_{56}H_{53}Cl_2N_5O_2Zn$: C 69.75, H 5.54, N 7.26; found C 69.58, H 5.43, N 7.10.

ZP-Cl$_4$PH: This compound was prepared in 9% yield by the condensation reaction of **ZPNH$_2$** with 3,4,5,6-tetrachlorophthalic anhydride. ^{1}H NMR ($CDCl_3$): $\delta = 10.34$ (s, 1H), 9.43 (d, $J = 5$ Hz, 2H), 9.14 (d, $J = 5$ Hz, 2H), 9.11 (d, $J = 5$ Hz, 2H), 9.07 (d, $J = 5$ Hz, 2H), 8.09 (d, $J = 2$ Hz, 4H), 7.84 (t, $J = 2$ Hz, 2H), 1.56 (s, 36H); UV (THF): $\lambda_{max} = 419$, 549, 590 nm;

fluorescence (THF, $\lambda_{ex} = 546$ nm): $\lambda_{em} = 593$, 650 nm; FAB MS: calcd for $C_{56}H_{51}Cl_4N_5O_2Zn$: 1029.2; found: 1029 [M^+].

ZP-PI: This compound was prepared in 44% yield by the condensation reaction of **ZPNH$_2$** with **1**. ^{1}H NMR ($CDCl_3$): $\delta = 10.36$ (s, 1H), 9.44 (d, $J =$ 5 Hz, 2H), 9.15 (d, $J = 5$ Hz, 2H), 9.12 (d, $J = 4$ Hz, 2H), 9.05 (d, $J = 5$ Hz, 2H), 8.69 (s, 2H), 8.09 (d, $J = 2$ Hz, 4H), 7.83 (t, $J = 2$Hz, 2H), 3.83 (t, 2H), 1.81 (m, 2H), 1.52 (s, 36H), 1.5 – 0.5 (m, 13H); UV (THF): $\lambda_{max} = 419$, 550, 589 nm; FAB MS: calcd for $C_{66}H_{70}N_6O_4Zn$: 1074.5; found: 1074 [M^+]; elemental analysis calcd (%) for $C_{66}H_{70}N_6O_4Zn$: C 73.62, H 6.55, N 7.81; found C 73.48, H 6.55, N 7.53.

ZP-NPH: This compound was prepared in 6% yield by the condensation reaction of **ZPNH$_2$** with 4-nitrophthalic anhydride. ^{1}H NMR ($CDCl_3$): $\delta =$ 10.36 (s, 1H), 9.44 (d, $J = 5$ Hz, 2H), 9.16 (d, $J = 5$ Hz, 2H), 9.12 (d, $J =$ 5 Hz, 2H), 9.10 (d, $J = 2$ Hz, 1H), 9.06 (d, $J = 5$ Hz, 2H), 8.92 (dd, $J = 2$, 8 Hz, 1H), 8.48 (d, $J = 8$ Hz, 1H), 8.09 (d, $J = 2$ Hz, 4H), 7.83 (t, $J = 2$ Hz, 2H), and 1.55 (s, 36H); UV (THF): $\lambda_{max} = 419$, 550, 590 nm; FAB MS: calcd for $C_{56}H_{54}N_6O_4Zn$: 938.3; found: 938 [M^+].

ZP-NI: This compound was prepared in 20% yield by the condensation reaction of **ZPNH$_2$** with **2**. ^{1}H NMR ($CDCl_3$): $\delta = 10.33$ (s, 1H), 9.43 (d, $J =$ 5 Hz, 2H), 9.13 (d, $J = 5$ Hz, 2H), 9.11 (d, $J = 5$ Hz, 2H), 9.06 (d, $J = 5$ Hz, 2H), 9.01 (d, $J = 8$ Hz, 2H), 8.95 (d, $J = 8$ Hz,2H), 8.07 (d, $J = 2$ Hz, 4H), 7.81 (t, $J = 2$ Hz, 2H), 4.30 (t, $J = 8$ Hz, 2H), 1.84 (m, 2H), 1.53 (s, 36H), 1.5 – 0.8 (m, 13H); UV (THF): $\lambda_{max} = 419$, 550, 589 nm; FAB MS: calcd for $C_{70}H_{72}N_6O_4Zn$: 1124.5; found: 1125 [M^+].

ZP-F$_4$PA: This compound was prepared in 3% yield by the condensation reaction of **ZPNH$_2$** with 3,4,5,6-tetrafluorophthalic anhydride. ^{1}H NMR ($CDCl_3$): $\delta = 10.31$ (d, $J = 12$Hz, 1H), 10.30 (s, 1H), 9.41 (d, $J = 5$ Hz, 2H), 9.40 (d, $J = 5$ Hz, 2H), 9.13 (d, $J = 5$ Hz, 2H), 9.11 (d, $J = 5$ Hz, 2H), 8.10 (d, $J = 2$ Hz, 4H), 8.06 (s, 1H), 7.84 (t, $J = 2$ Hz, 2H), 1.56 (s, 36H); UV (THF): $\lambda_{max} = 400$, 419, 551 nm; fluorescence (THF, $\lambda_{ex} = 419$ nm): $\lambda_{em} = 597$, 647 nm; FAB MS: calcd for $C_{55}H_{53}F_4N_5OZn$: 939.3; found: 939 [M^+].

Acknowledgements

This work was supported by Grant-in-Aid for Scientific Research (No. 11223205 and No. 12440196) from the Ministry of Education, Science, Sports and Culture of Japan and by CREST (Core Research for Evolutional Science and Technology) of Japan Science and Technology Corporation (JST). The work at Yonsei University was financially supported by the Creative Research Initiatives Program of the Ministry of Science and Technology of Korea. N. Y. is grateful for a JSPS Research Fellowship for Young Scientists. We are grateful to Prof. Noboru Mataga for useful suggestion.

[1] a) R. A. Marcus, *J. Chem. Phys.* **1956**, *24*, 966; b) R. A. Marcus, N. Sutin, *Biochim. Biophys. Acta* **1985**, *811*, 265.

[2] a) M. R. Wasielewski, *Chem. Rev.* **1992**, *92*, 435; b) G. L. Closs, J. R. Miller, *Science* **1988**, *240*, 440; c) A. Osuka, N. Mataga, T. Okada, *Pure Appl. Chem*. **1997**, *69*, 797.

[3] a) L. T. Calcaterra, G. L. Closs, J. R. Miller, *J. Am. Chem. Soc.* **1983**, *105*, 670; b) J. R. Miller, L. T. Calcaterra, G. L. Closs, *J. Am. Chem. Soc.* **1984**, *106*, 3047; c) G. L. Gaines III, M. P. O'neil, W. A. Svec, M. P. Niemczyk, M. R. Wasieleswki, *J. Am. Chem. Soc.* **1991**, *113*, 719; d) F. Pöllinger, C. Musewald, H. Heitele, M. E. Michel-Beyerle, C. Anders, M. Futscher, G. Voit, H. A. Staab, *Ber. Bunsenges. Phys. Chem*. **1996**, *100*, 2076; e) T. Häberle, J. Hirsch, F. Pöllinger, H. Heitele, M. E. Michel-Beyerle, C. Anders, A. Döhling, C. Krieger, A. Rückemann, H. A. Staab, *J. Phys. Chem*. **1996**, *100*, 18269.

[4] a) T. Asahi, M. Ohkohchi, R. Matsusaka, N. Mataga, R. P. Zhang, A. Osuka, K. Maruyama, *J. Am. Chem. Soc.* **1993**, *115*, 5665; b) A. Osuka, R. P. Zhang, K. Maruyama, I. Yamazaki, Y. Nishimura, *Bull. Chem. Soc. Jpn*. **1992**, *65*, 2807; c) M. Ohkohchi, A. Takahashi, N. Mataga, T. Okada, A. Osuka, H. Yamada, K. Maruyama, *J. Am. Chem. Soc.* **1993**, *115*, 12137.

[5] A. Osuka, G. Noya, S. Taniguchi, T. Okada, Y. Nishimura, I. Yamazaki, N. Mataga, *Chem. Eur. J.* **2000**, *6*, 33.

[6] a) N. Mataga, H. Miyasaka, *Prog. Reaction Kinet.* **1994**, *19*, 317; b) N. Mataga, H. Miyasaka, *Electron Transfer: From Isolated Molecules to Biomolecules*, *Vol. 107* (Eds.: J. Jortner, M. Bixon), Advances in Chemical Physics Series, Wiley, New York, **1999**, pp. 431.

[7] a) T. Asahi, N. Mataga, *J. Phys. Chem.* **1989**, *93*, 6575; b) T. Asahi, N. Mataga, Y. Takahashi, T. Miyashi, *Chem. Phys. Lett.* **1990**, *171*, 309; c) T. Asahi, N. Mataga, *J. Phys. Chem.* **1991**, *95*, 1956; d) T. Asahi, M. Ohkohchi, M. Nataga, *J. Phys. Chem.* **1993**, *97*, 13132; e) H. Miyasaka, S. Kotani, A. Itaya, *J. Phys. Chem.* **1995**, *99*, 5757; f) H. Miyasaka, S. Kotani, A. Itaya, G. Schweitzer, F. C. DeSchryver, N. Mataga, *J. Phys. Chem. B* **1997**, *101*, 7978.

[8] Quite recently, the synthesis and intramolecular ET reaction of Zn^{II} porphyrin-pyromellitimide (**ZP-PI** according to abbreviation used in this paper) have been reported: N. P. Redmore, I. V. Rubtsov, M. J. Therien, *Inorg. Chem.* **2002**, *41*, 570.

[9] a) A. Osuka, S. Nakajima, K. Maruyama, N. Mataga, T. Asahi, *Chem. Lett.* **1991**, 1003; b) A. Osuka, H. Yamada, K. Maruyama, N. Mataga, T. Asahi, I. Yamazaki, Y. Nishimura, *Chem. Phys. Lett.* **1991**, *181*, 419; c) A. Osuka, S. Nakajima, K. Maruyama, N. Mataga, T. Asahi, I. Yamazaki, Y. Nishimura, T. Ohno, K. Nozaki, *J. Am. Chem. Soc.* **1993**, *115*, 4577; d) A. Osuka, R.-P. Zhang, K. Maruyama, T. Ohno, K. Nozaki, *Bull. Chem. Soc. Jpn.* **1993**, *66*, 3773; e) G. P. Wiederrecht, M. P. Niemczyk, W. A. Svec, M. R. Wasielewski, *J. Am. Chem. Soc.* **1996**, *118*, 81.

[10] a) N. Mataga, H. Chosrowjan, Y. Shibata, N. Yoshida, A. Osuka, T. Kikuzawa, T. Okada, *J. Am. Chem. Soc.* **2001**, *123*, 12422; b) N. Mataga, H. Chosrowjan, S. Taniguchi, Y. Shibata, N. Yoshida, A. Osuka, T. Kikusawa, T. Okada, *J. Phys. Chem. A*, in press.

[11] a) H. Chosrowjan, S. Taniguchi, T. Okada, S. Takagi, T. Arai, K. Tokumaru, *Chem. Phys. Lett.* **1995**, *242*, 644; b) G. G. Gurzadyan, T.-H. Tran-Thi, T. Gustavsson, *J. Chem. Phys.* **1998**, *108*, 385; c) D. LeGourrierec, M. Andersson, J. Davidsson, E. Mukhtar, L. Sun, L. Hammarström, *J. Phys. Chem. A* **1999**, *103*, 557; d) S. Akimoto, T. Yamazaki, I. Yamazaki, A. Osuka, *Chem. Phys. Lett.* **1999**, *309*, 177; e) N. Mataga, Y. Shibata, H. Chosrowjan, N. Yoshida, A. Osuka, *J. Phys. Chem. B* **2000**, *104*, 4001; f) H. S. Cho, N. W. Song, Y. H. Kim, S. C. Jeoung, S. Hahn, D. Kim, S. K. Kim, N. Yoshida, A. Osuka, *J. Phys. Chem. A* **2000**, *104*, 3287.

[12] a) A. P. de Silva, H. Q. N. Gunaratne, T. Gunnlaugsson, A. J. M. Huxley, C. P. McCoy, J. T. Rademacher, T. E. Rice, *Chem. Rev.* **1997**, *97*, 1515; b) L. Fabbrizzi, M. Licchelli, P. Pallavicini, *Acc. Chem. Res.* **1999**, *32*, 846; c) R. T. Hayes, M. R. Wasielewski, D. Gosztola, *J. Am. Chem. Soc.* **2000**, *122*, 5563; d) C. P. Collier, G. Matterstei, E. W. Wong, Y. Luo, K. Beverly, J. Sampaio, F. M. Raymo, J. F. Stoddart, J. R. Heath, *Science* **2000**, *289*, 1172.

[13] a) A. P. de Silva, H. Q. N. Gunaratne, C. P. McCoy, *Nature* **1993**, *364*, 42; b) A. P. de Silva, H. Q. N. Gunaratne, G. E. M. Maguire, *Chem. Commun.* **1994**, 1213; c) A. P. de Silva, H. Q. N. Gunaratne, C. P. McCoy, *J. Am. Chem. Soc.* **1997**, *119*, 7891; d) A. Credi, V. Balzani, S. J. Langford, J. F. Stoddart, *J. Am. Chem. Soc.* **1997**, *119*, 2679; e) A. S. Lukas, P. J. Bushard, M. R. Wasielewski, *J. Am. Chem. Soc.* **2001**, *123*, 2440.

[14] a) J. Dalton, L. R. Milgrom, *J. Chem. Soc. Chem. Commun.* **1979**, 609; b) A. Harrimann, R. J. Hosie, *J. Photochem*. **1981**, *15*, 163; c) M. A. Bergkamp, J. Dalton, T. L. Netzel, *J. Am. Chem. Soc*. **1982**, *104*, 253; d) J. Rodriguez, C. Kirmaier, M. R. Johnson, R. A. Friesner, D. Holten, J. L. Sessler, *J. Am. Chem. Soc*. **1991**, *113*, 1652; e) K. Kamioka, R. A. Cormier, T. W. Lutton, J. S. Connolly, *J. Am. Chem. Soc*. **1992**, *114*, 4414; f) F. D'Souza, G. R. Deviprasad, Y.-Y. Hsieh, *Chem. Commun.* **1997**, 533; g) A. N. Macpherson, P. A. Liddell, S. Lin, L. Noss, G. R. Seely, J. M. DeGraziano, A. L. Moore, T. A. Moore, D. Gust, *J. Am. Chem. Soc.* **1995**, *117*, 7202.

[15] K. Wynne, S. M. LeCours, C. Galli, M. J. Therien, R. M. Hochstrasser, *J. Am. Chem. Soc*. **1995**, *117*, 3749.

[16] a) J. E. Baldwin, J. F. Debernardis, *J. Org. Chem.* **1977**, *42*, 3986; b) K. M. Smith, G. H. Barnett, B. Evans, Z. Martynenko, *J. Am. Chem. Soc*. **1979**, *101*, 5953; c) J. E. Baldwin, M. J. Crossley, J. F. Debernardis, *Tetrahedron* **1982**, *38*, 685.

[17] a) A. Osuka, H. Shimidzu, *Angew. Chem.* **1997**, *109*, 93; *Angew. Chem. Int. Ed. Engl*. **1997**, *36*, 135; b) N. Aratani, A. Osuka, Y. H. Kim, D. H. Jeong, D. Kim, *Angew. Chem.* **2000**, *112*, 1517; *Angew. Chem. Int. Ed.* **2000**, *39*, 1458.

[18] P. G. Seybold, M. Goutermann, *J. Mol. Spectrosc*. **1969**, *31*, 1.

[19] H. Miyasaka, T. Moriyama, A. Itaya, *J. Phys. Chem.* **1996**, *100*, 12609.

[20] A. Nakano, Y. Yasuda, T. Yamazaki, S. Akimoto, I. Yamazaki, H. Miyasaka, A. Itaya, M. Murakami, A. Osuka, *J. Phys. Chem. A* **2001**, *105*, 4822.

[21] A. Weller, *Z. Phys. Chem. (N.Y.)* **1982**, *133*, 93; in the Equation (5), r_D and r_A are the effective radii of $\mathbf{ZP}^+$ (5 Å) and acceptor (3.5 Å for $\mathbf{NI}^-$ and $\mathbf{PI}^-$, and 3 Å for other imide anions),[9] respectively, r is the center-to-center distance between donor and acceptor (8.4 Å for $\mathbf{ZP}^+-\mathbf{NI}^-$ and $\mathbf{ZP}^+-\mathbf{PI}^-$; 7.5 Å for other ion pairs), and ε_s is the dielectric constant of the solvent used for the transient absorption experiments and ε_r is the dielectric constant of DMF in which E_{ox} and E_{red} have been determined. In the present case, we have calculated the correction term ΔG_s; 0.17 eV in toluene, 0.08 eV in THF.

[22] a) H. Heitele, F. Pöllinger, T. Häberle, M. E. Michel-Beyerle, H. A. Staab, *J. Phys. Chem.* **1994**, *98*, 7402; b) J. M. DeGraziano, A. N. Macpherson, P. A. Liddell, L. Noss, J. P. Sumida, G. R. Seely, J. E. Lewis, A. L. Moore, T. A. Moore, D. Gust, *New J. Chem.* **1996**, *20*, 839; c) A. Osuka, S. Marumo, N. Mataga, S. Taniguchi, T. Okada, I. Yamazaki, Y. Nishimura, T. Ohno, K. Nozaki, *J. Am. Chem. Soc.* **1996**, *118*, 155.

[23] M. L. Horng, J. Gardecki, J. A. Papazyan, M,. Maroncelli, *J. Phys. Chem.* **1995**, *99*, 17311.

[24] J. M. DeGraziano, P. A. Liddell, L. Legget, A. L. Moore, T. A. Moore, D. J. Gust, *Phys. Chem.* **1994**, *98*, 1758.

[25] W. B. Davis, W. A. Svec, M. A. Ratner, M. R. Wasielewski, *Nature* **1998**, *396*, 60.

[26] B. C. Perung, M. D. Newton, F. O. Raineri, H. L. Friedman, *J. Chem. Phys.* **1996**, 1*04*, 7177.

[27] a) R. Englman, J. Jortner, *Mol. Phys.* **1970**, *18*, 145; b) K. F. Freed, J. Jortner, *J. Chem. Phys.* **1970**, *52*, 6272.

[28] R. Kubo, Y. Toyozawa, *Prog. Theor. Phys.* **1955**, *13*, 160.

[29] P. Chen, S. L. Mecklenburg, T. J. Meyer, *J. Phys. Chem.* **1993**, *97*, 13126.

[30] M. Lee, D. Kim, *J. Opt. Soc. Korea* **1990**, *1*, 52.

Received: November 19, 2002 [F4588]